Syntheses of Highly Ordered Mesoporous Materials, FSM-16, Derived from Kanemite

Shinji Inagaki,* Akihiko Koiwai, Noritomo Suzuki, Yoshiaki Fukushima, and Kazuyuki Kuroda†

Toyota Central R&D Labs., Inc., 41-1, Yokomichi, Nagakute-cho, Aichi 480-11

†Department of Applied Chemistry, Waseda University, Ohkubo-3, Shinjuku-ku, Tokyo 169

(Received January 5, 1996)

The synthetic conditions of highly ordered and thermally stable mesoporous molecular sieves from a layered silicate kanemite are established. We divided the formation process of the mesoporous materials from kanemite into two elemental processes: i) exchange of Na^+ in the interlayer of kanemite for alkyltrimethylammonium cations and ii) condensation of silicates and formation of a three dimensional silicate framework. Higher pH (over 11.5) at the cation-exchange process and the subsequent pH adjustment at 8.5 at the condensation process were best suited for the formation of mesoporous products with high regularity and thermal stability. Removal of partially dissolved kanemite during the cation-exchange process avoided the formation of amorphous materials as a by-product. Structures of some intermediate silicate/surfactant complexes supported the proposed folded sheets mechanism for the formation of the mesoporous molecular sieves. Syntheses by using alkyltrimethylammonium with different alkyl-chain lengths are also reported.

The syntheses of highly ordered mesoporous molecular sieves have attracted much attention in recent years. Yanagisawa et al.[1] reported syntheses of mesoporous silicas with uniform pore sizes from a layered polysilicate, kanemite,[2] in 1988. It was suggested that the silicate single layers[3] of kanemite condense to form a three-dimensional silicate network during cation-exchange of Na^+ ions in the interlayer of kanemite for alkyltrimethylammonium ions.[4] The pore size could be controlled by using alkyltrimethylammonium ions with different alkylchain lengths. Yanagisawa et al.[5] also reported precise pore size control of the mesoporous silica by trimethylsilylation. Inagaki et al.[6] reported the addition of acidity by incorporation of aluminum in the silica framework and revealed that the acidic property was similar to that of the usual amorphous silica-alumina. However, the pore arrangement of the mesoporous materials derived from kanemite appeared not so regular as those in zeolites.

Researchers at Mobil[7—10] reported a family of mesoporous materials (M41S) with a regular arrangement of mesopores. They proposed a liquid-crystal template (LCT) model for the formation mechanism.[8] MCM-41, one member of this family, exhibits a hexagonal arrangement of uniform mesopores whose dimensions could be changed between ca. 1.5 and 10 nm.

Modifying the reaction conditions for the formation of mesoporous silica from kanemite also yielded a highly ordered one with a hexagonal arrangement of the channels.[11] We have proposed a folded sheets formation mechanism[12] of the highly ordered mesoporous materials from kanemite and called them FSM (Folded Sheets Mesoporous materials). The materials was designated as FSM-16.

Monnier et al.[13] observed the formation of a lamellar surfactant-silicate mesophase in the initial 20 min of the synthesis of MCM-41 and its transformation to a hexagonal mesophase.[14] The similar mechanism via a lamellar intermediate mesophase to form a MCM-41 material has also been proposed by another group.[15] Chen et al.[16] reported that the above two types of materials, MCM-41 and FSM-16, were formed by different mechanisms and the materials derived from kanemite had higher thermal and hydrothermal stability than MCM-41. They reported, however, that the materials produced at the condition of higher kanemite-to-solution ratio=1 : 20,[11,12] which resulted in a higher pH (>11.5) of reaction mixture, were formed by the LCT mechanism because of the dissolution of kanemite. Vartuli et al.[17] also compared both materials and reported that they had different formation pathways and that MCM-41 materials had 5 times larger adsorption capacities than those of the mesoporous materials derived from kanemite. O'Brien et al.[18] reported that real-time in situ X-ray powder diffraction data provided evidence for the formation of an intermediate lamellar silica-surfactant intercalate during the syntheses of the hexagonal mesophase derived from kanemite, whereas no intermediate phases were observed during the formation of mesophase that leaded to MCM-41.

The process to produce the mesoporous materials from kanemite can be divided into two elementary processes: i) exchange of Na^+ in the interlayer of kanemite for alkyltrimethylammonium cations and ii) condensation of silicates and forming a three dimensional silicate framework. The cation-exchange property of kanemite and the condensation of silicates would be affected by the pH of the reaction solution. Here we study the effect of pH at the elementary processes on the formation of highly regular and thermally

stable FSM-16 materials and we discuss the folded sheets formation mechanism.

Experimental

Materials. A spray-dried sodium silicate water-glass powder, whose SiO_2/Na_2O ratio was adjusted at 2.00, was supplied by Nippon Kagaku Kogyo Corp. Alkyltrimethylammonium $[C_nH_{2n+1}N^+(CH_3)_3]$ bromide (n=8, 10 and 12) and chloride (n=14, 16 and 18) were obtained from Tokyo Kasei and used without further purification.

Preparation of Kanemite. The sodium silicate powder was calcined at 700 °C for 6 h to obtaine δ-$Na_2Si_2O_5$ crystal. Fifty grams of δ-$Na_2Si_2O_5$ powder was dispersed in 500 cm^3 of distilled water and stirred for 3 h at room temperature. Filtration of the dispersion gave us a wet kanemite paste. The wet kanemite was used for the next cation-exchange process without drying. X-Ray powder diffraction of the dried sample confirmed the formation of the kanemite. The composition of the kanemite was $Na_{1.6}H_{0.4}Si_2O_5 \cdot nH_2O$, which was determined by atomic absorption spectrometer (AAS) for Na and inductively coupled plasma-atomic emission spectrometer (ICP-AES) for Si.

Variation of pH during Cation-Exchange Process. The wet kanemite corresponding to 50 g of dried kanemite was dispersed in a 1000 cm^3 of a 0.1 mol dm^{-3} hexadecyltrimethylammonium (HDTMA) chloride solution. The pH of the suspension was adjusted to the appropriate values (7, 8.5, 10, 11.5, and 12.3) by adding a 2 mol dm^{-3} HCl aqueous solution. The pH adjusted suspensions were heated at 70 °C for 3 h under stirring in a 2000 cm^3 flask and the pH was kept in a range $\pm$ 0.5 around the appropriate values during the heating. After cooling to room temperature, the solid products were separated from the solutions by filtration. The filtered solid products were dispersed in 1000 cm^3 water again and the pH of the suspension was adjusted at 8.5 by the addition of a 2 mol dm^{-3} HCl aqueous solution slowly. After stirring for 1 h at room temperature the solid products were filtered, washed with 1000 cm^3 water five times and air-dried to yield silicate/organic complexes.

Preparation of Intermediate Complexes. Figure 1 shows an optimal synthetic procedure of FSM-16. Some intermediate silicate/organic complexes were prepared as shown in Fig. 1. The wet kanemite prepared by dispersion of 20 g of δ-$Na_2Si_2O_5$ in 200 cm^3 of water was dispersed in a 400 cm^3 volume of 0.1 mol dm^{-3} HDTMA chloride solution. The pH of the suspension was 12.3. The suspension was heated at 70 °C for 3 h under stirring in a 1000 cm^3 flask. After cooling to room temperature, the solid product was separated from the solution by filtration. The filtered product was washed with 400 cm^3 distilled water five times and air-dried to yield the intermediate sample A. The other filtered products were dispersed in 400 cm^3 water and the pH of the suspension was adjusted at 8.5 by the addition of a 2 mol dm^{-3} HCl aqueous solution slowly. After the dispersion was stirred for 3 h at room temperature, the solid product was filtered, washed with 400 cm^3 distilled water five times and air-dried to yield the intermediate B. Intermediates C and D were prepared by heating the intermediate B in water at 70 °C for 3 and 48 h, respectively. All these samples were calcined at 550 or 900 °C for 6 h in air.

Residual Na, Al, and Fe contents in the calcined product of the sample D were 0.14, 0.02, and 0.02 wt% respectively, which were determined by AAS for Na and ICP-AES for Al and Fe.

Syntheses by Using Surfactants with Different Alkyl-Chain Length. The wet kanemite prepared by dispersing 50 g of δ-$Na_2Si_2O_5$ in 500 cm^3 of water was dispersed in a 1000 cm^3 solution of 0.1 mol dm^{-3} alkyltrimethylammonium $[C_nH_{2n+1}N^+(CH_3)_3]$ with different alkyl-chain lengths (n). After the suspensions were heated at 70 °C for 3 h, the pH of the dispersion was adjusted at 8.5 by addition of a 2 mol dm^{-3} HCl aqueous solution. After heating for further 3 h, the suspensions were cooled to room temperature. Filtered solid products were washed five times with 1000 cm^3 distilled water and air-dried, followed by calcination at 550 °C for 6 h in air.

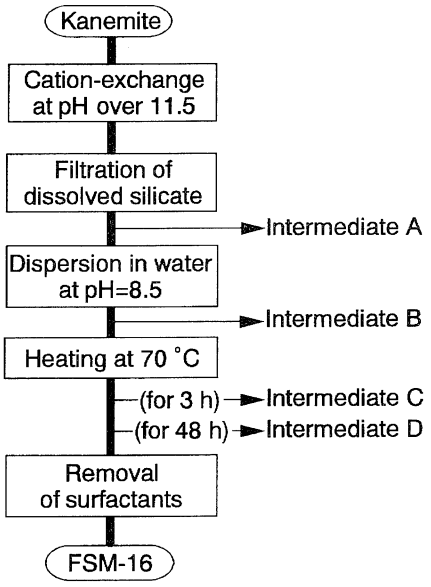

Fig. 1. Synthetic procedures of FSM-16 and the intermediate silicate/organic complexes.

Characterization. X-Ray powder diffraction (XRD) patterns were obtained by using a Rigaku RAD-B diffractometer with Cu $K\alpha$ radiation. Solid state ^{29}Si MAS NMR spectra were recorded on a Bruker MSL-300WB spectrometer at 59.620 MHz spinning 4 kHz using pulses at 90-s intervals. A peak intensity was not changed when the pulse intervals were over 90-s. N_2 adsorption–desorption isotherms at −196 °C were measured by means of volumetrical method using a conventional vacuum-line with a Baratron pressure transducer (127AA) and controlled valves (248A). Tentative pore diameters were calculated by the correct Kelvin equation, in which a multilayer adsorption was taken into consideration, using the P/P_0 positions of inflection on the adsorption isotherm due to filling nitrogen within the pores. The thicknesses of the multilayer adsorption were estimated from adsorption data of nitrogen on non-porous silica reported by Bhambhani et al.[19] Specific surface areas were calculated by BET method using the adsorption data at the range from P/P_0=0.05 to P/P_0 just below the capillary condensation. Pore volumes were obtained from the saturated adsorption amount of nitrogen by assuming that each pore was filled with condensed liquid nitrogen. Transmission electron micrographs (TEM) were obtained with a JEOL JEM-200CX at an accelerating voltage of 200 kV. Powdered sample of the intermediate D was observed directly on a Cu-mesh by TEM. The calcined product was buried in epoxy resins and sectioned for TEM observation. Elemental analyses of organic matters were obtained by a Perkin–Elmer 240C elemental-analyzer.

Results

Effect of pH during Cation-Exchange Process. Figure 2 shows X-ray diffraction patterns of the silicate/organic complexes prepared by heating kanemite in HDTMA so-

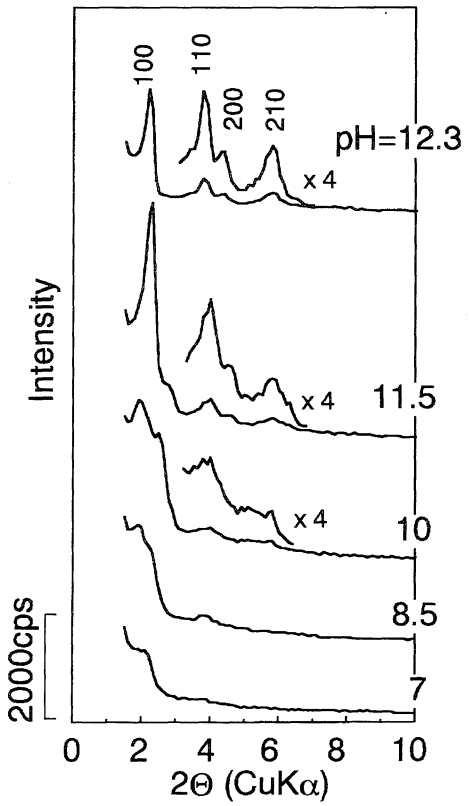

Fig. 2. XRD patterns of the silicate/HDTMA complexes prepared at various pH.

lutions at various pH values. The complexes prepared at pH of 11.5 and 12.3 show four diffraction peaks assigned to hexagonal regularity. A decrease in the pH weakened the diffraction peaks. The results of elemental analyses (Table 1) show that the HDTMA/SiO_2 ratio in the complexes increased with pH. Increasing the pH increased the cation-exchange ratio of Na^+ ions in the interlayer of kanemite for HDTMA cations and the hexagonal regularity.

Table 2 lists the yields of the silicate/organic complexes and Si mass balances between kanemite and the products. Although the yield was not affected by the pH values, the Si mass balance decreased with increasing pH. This is attributable to partial dissolution of kanemite during the cation exchange reaction at higher pH. The dissolved silicates were removed from the residual products by filtration before pH adjustment. The ^{29}Si MAS NMR spectra of the complexes

Table 1. Elemental Analyses of Silicate/HDTMA Complexes Prepared at Various pH

pH	wt%				HDTMA /SiO_2 (mol/mol)
	C	H	N	Ash (960 °C)	
7.0	15.69	3.45	0.94	68.88	0.060
8.5	17.34	3.71	1.01	66.03	0.069
10.0	32.46	6.70	2.00	48.08	0.178
11.5	38.57	7.90	2.37	39.21	0.259
12.3	40.84	8.12	2.45	35.01	0.308

Table 2. Yields of the Silicate/HDTMA Complexes Prepared at Various pH and Mass Balances of Si

pH	Yields of as-synthesized	Weight of Si[a)] in the yields	Mass balances[b)] of Si
	g	g	%
7.0	32	10.3	68
8.5	42	13.0	86
10.0	46	10.3	68
11.5	36	6.6	43
12.3	33	5.4	36

a) Si contents were determined from ash of elemental analyses.
b) Weight of Si in 50 g of kanemite was 15.2 g.

in Fig. 3 had two broad signals which were assignable to Q^4 (from 107.3 to 111.5 ppm) and Q^3 (from 97.8 to 101.2 ppm) units. The intensity ratio of Q^4 to Q^3 signals increased with decreasing the pH. These results indicated that condensation between SiO_4-sheets of kanemite occurred during the lower pH treatment. The condensation in higher degree would also prevent the cation-exchange for surfactants ions and the formation of the higher hexagonal regularity.

Effect of pH-Adjustment after Cation Exchange at pH=12.3. Figure 4 shows XRD patterns and ^{29}Si MAS NMR spectra of kanemite and the intermediates A, B, C, and D. As kanemite has a single sheet structure, only a sharp Q^3 signal was observed. The intermediate A also had

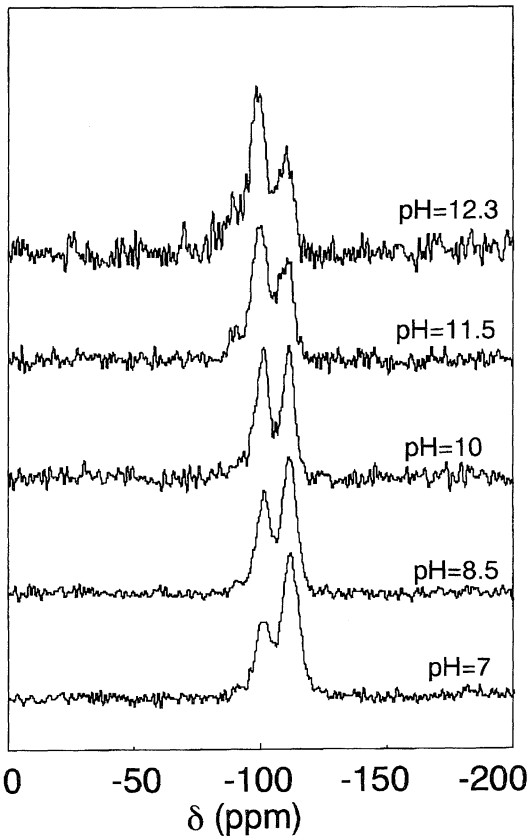

Fig. 3. ^{29}Si MAS NMR spectra of the silicate/HDTMA complexes prepared at various pH.

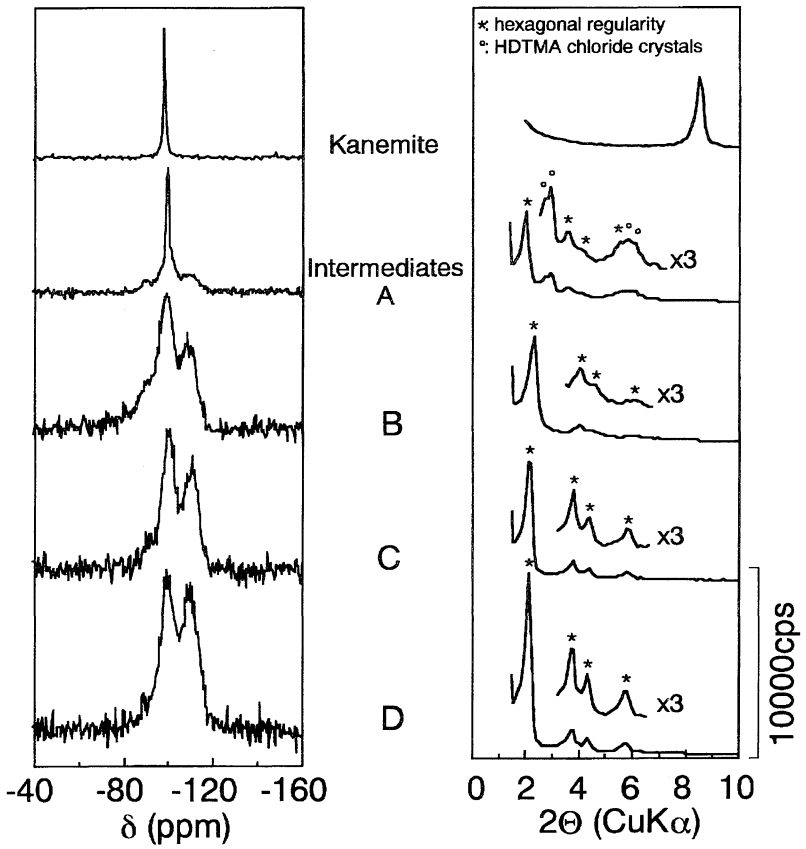

Fig. 4. ^{29}Si MAS NMR spectra and XRD patterns of kanemite and the intermediate silicate/HDTMA complexes A, B, C, and D.

a sharp Q^3 signal with a weak Q^4 signal, indicating that the sheet structure of kanemite was largely retained. However, the complex A did not show a layered structure but hexagonal regularity, as shown in XRD patterns in Fig. 4. Small diffraction peaks due to HDTMA chloride crystals were also observed for the sample A. The signal of Q^4 silicon sites appeared obviously for the sample B and both of the Q^3 and Q^4 signals were broadened. The XRD pattern for the sample B showed only peaks due to hexagonal regularity. The diffraction peaks and the ratio of Q^4/Q^3 intensity in ^{29}Si MAS NMR spectra were enhanced for the samples C and D.

The lattice parameters determined from d-spacing of 100 reflections of the XRD patterns are listed in Table 3. The intermediate A had the largest lattice parameter of a=4.77 nm, and those of the intermediates B, C, and D were 4.39, 4.61, and 4.68 nm, respectively.

Structure of the Calcined Samples. Figure 5 shows the XRD patterns of the calcined intermediate samples at 550 and 900 °C. Although the diffraction peaks almost disappeared for the sample A, the samples B, C, and D retained the peaks after calcination at 550 °C. Sample D still exhibited the diffraction peaks even after calcination at 900 °C. The hexagonal structure of the calcined samples was steady in the order of sample A, B, C, and D. The peak intensity of the sample D increased 2.5 times upon calcination at 550 °C. The lattice parameters decreased with calcination temperature as listed in Table 3. The extent of shrinkage (Δ) in the lattice parameter decreased in the order of the intermediates B, C, and D, that is the same as the order of hexagonal regularity. The extent of shrinkage in the intermediate D was 0.33 nm after calcination at 550 °C and 0.73 nm after calcination at 900 °C.

Table 3. Unit Cell Dimensions of the Intermediates and the Calcined Samples

Intermediate samples	Unit cell dimensions (Δ[a])/nm		
		Calcined at	
	Uncalcined	550 °C	900 °C
A	4.77	—	—
B	4.39	3.88 (0.51)	3.44 (0.95)
C	4.61	4.25 (0.36)	3.76 (0.85)
D	4.68	4.35 (0.33)	3.95 (0.73)

a) Δ are differences of unit cell dimensions between uncalcined and calcined samples.

Nitrogen adsorption isotherms of the calcined products are shown in Fig. 6. The stepwise increase in adsorption at P/P_0 between 0.2 and 0.4 due to filling nitrogen within the mesopores became steeper in the order of sample A, B, C, and D, which indicated narrower pore size distribution. The tentative pore diameter (Table 4) of calcined intermediate sample D decreased from 2.6 to 2.1 nm with increase in the calcined temperature from 550 to 900 °C. The specific surface areas (Table 4) were 900—1100 $m^2\ g^{-1}$ for the calcined samples at 550 °C and 900 $m^2\ g^{-1}$ for the calcined sample D even at

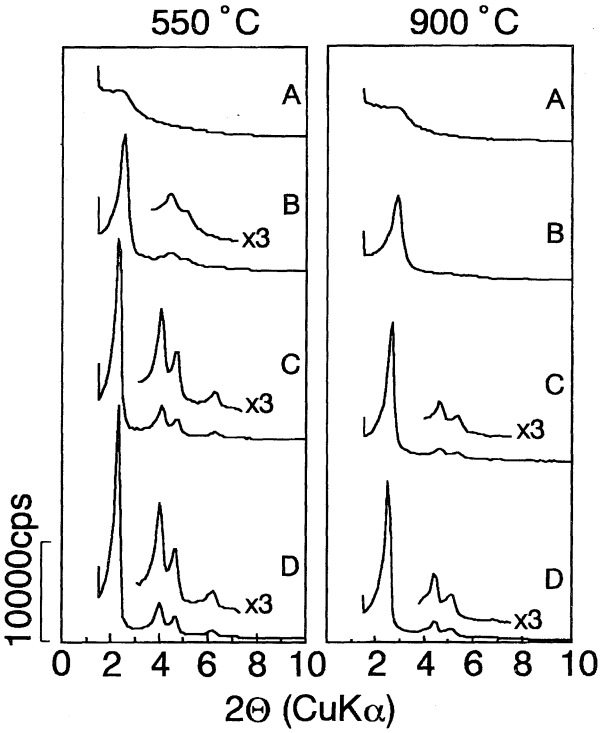

Fig. 5. XRD patterns of the calcined intermediate samples A, B, C, and D.

900 °C.

^{29}Si MAS NMR spectra (Fig. 7) of the calcined sample D showed a broad peak at −109 ppm with a shoulder peak at −101 ppm. The shoulder peak intensity decreased with increase in calcination temperature.

Table 4. Tentative Pore Diameters and BET Surface Areas of the Calcined Intermediate Samples

Calcined intermediate samples	Tentative pore diameters nm	Specific surface areas[a] $m^2 g^{-1}$
(at 550 °C)		
A	—	910
B	2.2	1094
C	2.5	968
D	2.6	1028
(at 900 °C)		
D	2.1	900

a) They were calculated by BET equation using adsorption data at P/P_0 between 0.05 and 0.2.

Electron Microscopic Observations. Transmission electron micrographs of the as-synthesized material and the calcined product at 550 °C are shown in Fig. 8. A regular honeycomb like arrangement of channels with uniform size were observed for the both samples (Fig. 8, a and b). The pore walls of the calcined sample (Fig. 8, b) were thicker than those of the as-synthesized material (Fig. 8, a). A section parallel to the channels (Fig. 8, c) showed slightly wound continuous channels and the channels length was more than

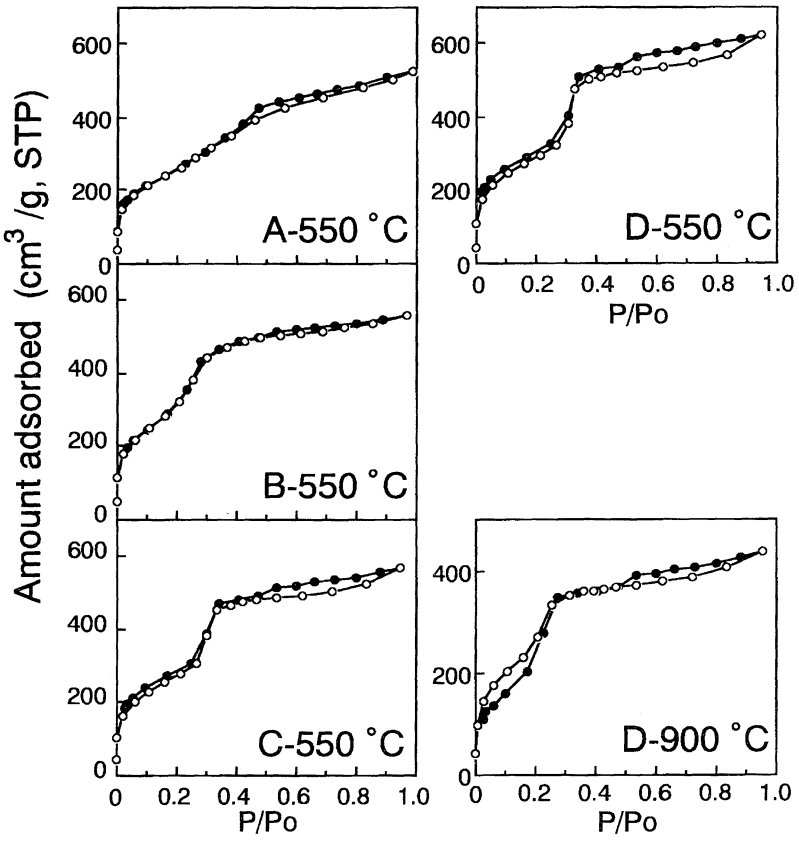

Fig. 6. N_2 adsorption/desorption isotherms of calcined intermediate samples A, B, C, and D.

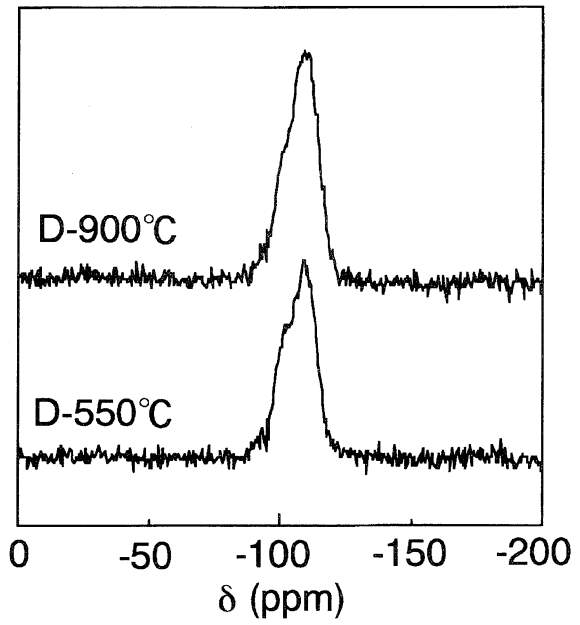

Fig. 7. ^{29}Si MAS NMR spectra of calcined samples (intermediate D).

0.5 mm.

Mesoporous Materials with Different Pore Sizes. Figure 9 shows XRD patterns of mesoporous materials prepared by using various surfactants with different alkyl-chain lengths (n). Although clear hexagonal patterns were observed for n=14, 16, and 18, the peaks became ambiguous for n=8, 10, and 12. Nitrogen adsorption isotherms of the calcined products at 550 °C had sharp increases in adsorption as shown in Fig. 10. The inflection position at which the adsorption amounts increased was shifted from <0.08 to 0.40 with increasing surfactant chain length.

Table 5 lists the unit cell dimensions, tentative pore diameters, specific surface areas, and pore volumes of the calcined products at 550 °C. Decreasing the chain length in the surfactants decreased unit cell dimension, tentative pore diameter, and pore volume. The specific surface area did not change with the chain length and was almost 1000 $m^2 g^{-1}$ for the samples ($10 \leq n \leq 18$).

Table 5. Unit Cell Dimensions, Tentative Pore Diameters, Specific Surface Areas and Pore Volumes of FSM-16 Prepared by Using Various Surfactants with Different Alkyl-Chain Lengths

Surfactant chain length $C_nH_{2n+1}N^+(CH_3)_3$	Unit cell dimensions	Tentative pore diameters	Specific surface areas[a)]	Pore volumes
n=	nm	nm	($m^2 g^{-1}$)	$cm^3 g^{-1}$
8	3.09	<1.5	680	0.28
10	3.28	1.6	999	0.47
12	3.68	2.0	923	0.53
14	3.90	2.3	1017	0.69
16	4.38	2.7	1031	0.80
18	4.90	3.2	929	0.83

a) The specific surface areas were calculated by BET equation using adsorption data at $0.05<P/P_0<0.1$ on n=8, $0.05<P/P_0<0.12$ on n=10, $0.05<P/P_0<0.15$ on n=12, $0.05<P/P_0<0.2$ on n=14, $0.05<P/P_0<0.25$ on n=16, and $0.05<P/P_0<0.35$ on n=18.

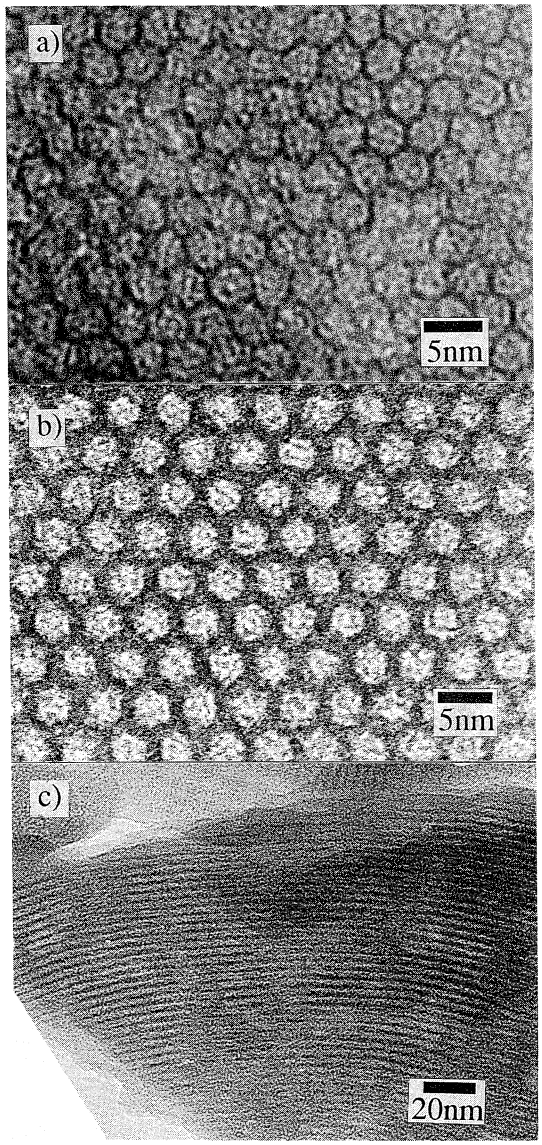

Fig. 8. Transmission electron micrographs of a) as-synthesized material and b, c) the calcined samples at 550 °C.

Discussion

We divided the formation of the mesoporous molecular sieves from kanemite into two elemental processes and optimized the pH conditions at each process. We consequently established the reaction conditions to produce the highly ordered and thermally stable mesoporous molecular sieves.

The Na^+ ions in kanemite were exchanged not only for organic surfactants but also for H^+.[20] As higher pH condition prevented the exchange for H^+, the higher pH ($\geq$11.5) was preferred for the cation-exchange process. The larger amount of exchanged surfactant ions in the interlayer affords the higher hexagonal regularity. The low adsorption capacity of the mesoporous material derived from kanemite reported by Vartuli et al.[17] is attributable to the low content of Na

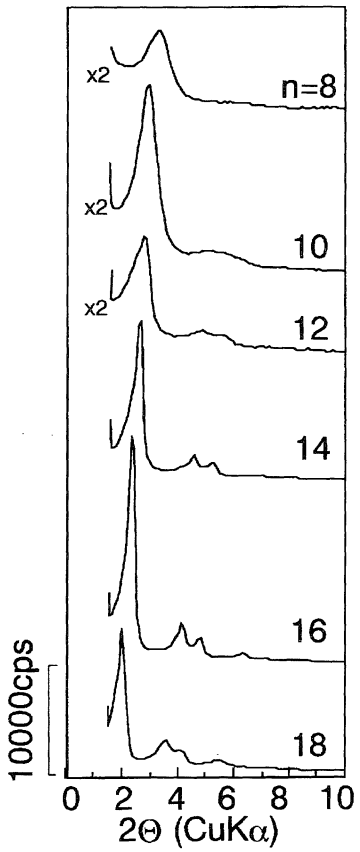

Fig. 9. XRD patterns of FSM-16 prepared by uisng various alkyltrimethylammonium ions with different alkyl-chain lengths (*n* are carbon numbers of alkyl-chains).

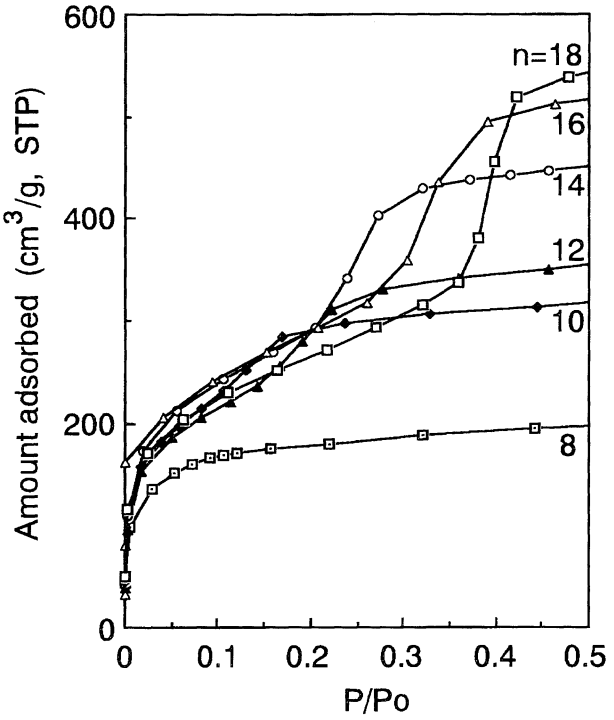

Fig. 10. N_2 adsorption isotherms of FSM-16 prepared by useing various alkyltrimethylammonium ions with different alkyl-chain lengths (*n* are carbon numbers of alkyl-chains).

in the kanemite as a starting material, whose composition was $Na_{0.4}H_{1.6}Si_2O_5$. The low content of Na ions caused low extent of exchange for surfactant ions and insufficient expansion of the interlayer of kanemite. Although high pH reaction condition promoted the dissolution of kanemite, we removed the dissolved species from the system by filtration before the pH adjustment at 8.5 and obtained only the solid products. In general, silicates can be easily condensed at around pH=7. The decrease in pH to 8.5 and a post-synthesis heat-treatment accelerated the condensation of silicates and formed a stable hexagonal framework with high regularity.

The large shrinkage of the lattice parameter after the calcination suggests a rearrangement of SiO_4 tetrahedra in the walls of the channels. The increase in the intensity of Q^4 signal and the peak broadening in ^{29}Si MAS NMR during calcination indicates increased condensation and distortion of the SiO_4 tetrahedra. A comparison of transmission electron micrographs of the materials before and after calcination suggests thickening of the pore walls during calcination. The lattice constant of MCM-41 as-synthesized material before and after calcination at 540 °C was 5.07 and 4.18 nm, respectively.[21] The larger lattice shrinkage for MCM-41 would be attributable to lower condensation ratio of the silicate species.[22]

These synthetic conditions of FSM-16 were more moderate than those of MCM-41. The most distinguished condition is the concentration of $HDTMA^+$ ions employed. In order to prepare typical MCM-41, a 26 wt% $HDTMA^+$ chloride solution was used[7,8,10,21] whereas the concentration of only 3.2 wt% aqueous solution was employed for preparing FSM-16. The reaction temperature for the formation of FSM-16 was 70 °C. On MCM-41, the reaction temperatures above 100 °C were normally employed to produce highly ordered MCM-41 materials. These moderate reaction conditions are attributable to utilizing a kanemite as the starting material for the formation of FSM-16. As a closed autoclave is usually used for the synthesis of zeolites or the M41S materials, pH conditions during the reaction cannot easily be adjusted. We changed the pH of the solution during the reaction to form a FSM-16. The pH adjustments during the syntheses allows a precise structure control of porous crystals. This method was useful for the rational synthesis of FSM-16 and could be applied to the syntheses of other inorganic materials such as zeolite, M41S materials and mesostructured transition-metal oxide compounds.[23]

Figure 11 shows our proposed structural models of the intermediate samples A, B, C, and D. It seems reasonable to describe the intermediate A as having a structure of surfactant aggregations among regularly waved silicate sheets. The ^{29}Si MAS NMR confirms that the ordering structure of SiO_4 tetrahedra in kanemite sheets is still preserved in the waved silicate sheets in the intermediate A. The hexagonal diffraction pattern observed in the intermediate A would be due to a regular fluctuation of surfactant aggregations in the interlayer of the waved silicates, although further studies are needed to confirm the structure of the intermediate A. The decrease in pH caused interlayer cross-linking and produced the

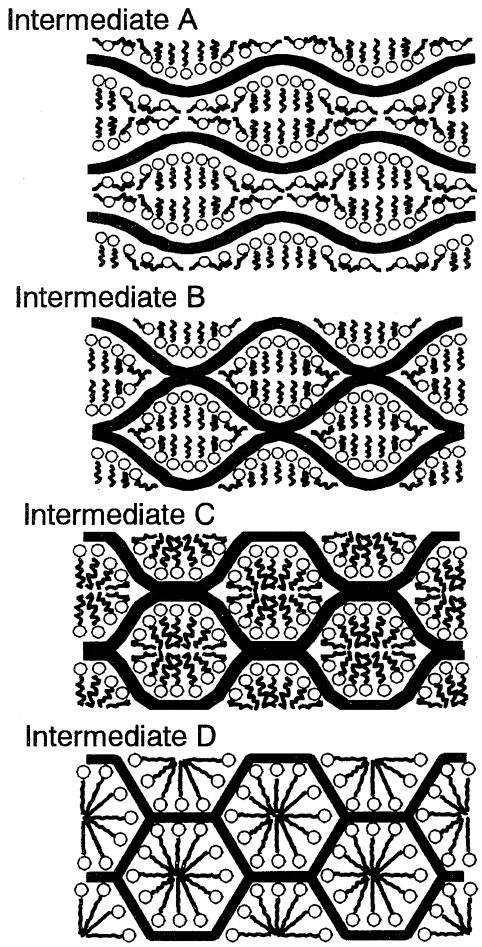

Fig. 11. Structural models of the intermediate silicate/surfactant complexes A, B, C, and D.

intermediate B. The interlayer cross-linking shrinks the lattice dimension and distorts the regular arrangement of SiO_4 tetrahedra in the silicate sheets of the intermediate A. Heat-treatment at 70 °C accelerates the interlayer cross-linking to form the intermediates C and D. Although the pH-adjustment and the heat-treatment distorted the arrangement of SiO_4 tetrahedra in the silicate sheets, they increased hexagonal regularity of the pore-arrangement. The increase in the lattice dimension with the heat-treatment was observed. Well-defined crystal structures of α-[24] and β-$Na_2Si_2O_5$[25] materials and the unit cell dimensions[2] of kanemite suggested that the silicate sheets of kanemite was slightly wrinkled. It would be regarded that rearrangements of surfactant molecules stretched the wrinkled silicate sheets and increased the lattice dimension.

A driving force for bending the silicate sheet of kanemite would be the aggregation force of surfactant ions. Kanemite concentrates surfactant ions in the interlayer from even a dilute surfactant solution and consequently induces aggregations of surfactants. The silicate sheets of kanemite would be easily folded because of its single layered structure. As the silicate sheets bond to the surfactants through ionic interaction, they are distorted by the surfactants.

The morphology of the FSM-16, which resembles the original kanemite,[11] was quite different from that of MCM-41 which showed particles shaped like a hexagonal prism. This is evidence for the topochemical folded sheet mechanism, as proposed. The LCT synthesis enables one to form cubic or lamellar phase materials at surfactants/Si ratios higher than 1.0.[10] No cubic phase materials form kanemite even at the ratio of surfactants to Si higher than 1.0.[26] This also supports a formation mechanism different from that of MCM-41.

The pore arrangement of FSM-16 is similar to that of MCM-41 as observed by XRD and TEM, although it seems that the pore wall structure of these materials are a little different. Benzene adsorption isotherms showed capillary condensation at 0.12—0.21 of P/P_0 for the FSM-16 samples with a=4.4 nm,[27] while P/P_0 value of 0.22—0.35 were required for benzene condensation for MCM-41 with a=4.0 nm.[8] These results suggest a different pore wall structure between FSM-16 and MCM-41 materials. The preservation of XRD patterns and uniform pore size distribution of FSM-16 at a high temperature of up to 900 °C indicates higher thermal and hydrothermal stability for FSM-16 than MCM-41 as reported by Chen et al.[16] The difference of thermal stability between these materials would also be attributable to the different pore wall structure.

References

1) T. Yanagisawa, T. Shimizu, K. Kuroda, and C. Kato, "56th National Meeting of the Chemical Society of Japan," Tokyo, April 1988, Abstr., I, pp. 761, No. IXIID42

2) Z. Johan and G. F. Maglione, *Bull. Soc. Fr. Mineral. Cristallogr.*, **95**, 371 (1972).

3) T. J. Pinnavaia, I. D. Johnson, and M. Lipsicas, *J. Solid State Chem.*, **63**, 118 (1986).

4) T. Yanagisawa, T. Shimizu, K. Kuroda, and C. Kato, *Bull. Chem. Soc. Jpn.*, **63**, 988 (1990).

5) T. Yanagisawa, T. Shimizu, K. Kuroda, and C. Kato, *Bull. Chem. Soc. Jpn.*, **63**, 1535 (1990).

6) S. Inagaki, Y. Fukushima, A. Okada, T. Kurauchi, K. Kuroda, and C. Kato, "In Proceedings from the Ninth International Zeolite Conference," ed by R. von Ballmoos, J. B. Higgins, and M. M. J. Treacy, Butterworth-Heinemann, London (1992), Vol. I, pp. 305—311.

7) C. T. Kresge, M. E. Leonowicz, W. J. Roth, J. C. Vartuli, and J. S. Beck, *Nature*, **359**, 710 (1992).

8) J. S. Beck, J. C. Vartuli, W. J. Roth, M. E. Leonowicz, C. T. Kresge, K. D. Schmitt, C. T-W. Chu, D. H. Olson, E. W. Sheppard, S. B. McCullen, J. B. Higgins, and J. L. Schlenker, *J. Am. Chem. Soc.*, **114**, 10834 (1992).

9) J. S. Beck, J. C. Vartuli, G. J. Kennedy, C. T. Kresge, E. J. Royh, and S. E. Schramm, *Chem. Mater.*, **6**, 1816 (1994).

10) J. C. Vartuli, K. D. Schmitt, C. T. Kresge, W. J. Roth, M. E. Leonowicz, S. B. McCullen, S. D. Hellring, J. S. Beck, J. L. Schlenker, D. H. Olson, and E. W. Sheppard, *Chem. Mater.*, **6**, 2317 (1994).

11) S. Inagaki, Y. Fukushima, and K. Kuroda, *J. Chem. Soc., Chem. Commun.*, 680 (1993).

12) S. Inagaki, Y. Fukushima, and K. Kuroda, "In Zeolite and Related Microporous Materials: State of the Art 1994," ed by J. Weitkamp, H. G. Karge, H. Pfeifer, and W. Holderich, Elsevier, Amsterdam (1994), pp. 125—132.

13) A. Monnier, F. Schuth, Q. Huo, D. Kumar, D. Margolese, R. S. Maxwell, G. D. Stucky, M. Krishnamurty, P. Petroff, A. Firouzi, M. Janicke, and B. F. Chmelka, *Science*, **261**, 1299 (1993).

14) V. Alfredsson, M. Keung, A. Monnier, G. D. Stucky, K. K. Unger, and F. Schuth, *J. Chem. Soc., Chem. Commun.*, 921 (1994).

15) A. Steel, S. W. Carr, and M. W. Anderson, *J. Chem. Soc., Chem. Commun.*, 1571 (1994).

16) C-Y. Chen, S-Q. Xiao, and M. E. Davis, *Microporous Mater.*, **4**, 1 (1995).

17) J. C. Vartuli, C. T. Kresge, M. E. Leonowicz, A. S. Chu, S. B. McCullen, I. D. Jonson, and E. W. Sheppard, *Chem. Mater.*, **6**, 2070 (1994).

18) S. O'Brien, R. J. Francis, S. J. Price, D. O'Hare, S. M. Clark, N. Okazaki, and K. Koroda, *J. Chem. Soc., Chem. Cummun.*, 2423 (1995).

19) M. R. Bhambhani, P. A. Cutting, K. S. W. Sing, and D. H. Turk, *J. Colloid Interface Sci.*, **38**, 109 (1972).

20) K. Beneke and G. Lagaly, *Am. Mineral.*, **62**, 763 (1977).

21) C-Y. Chen, H-X. Li, and M. E. Davis, *Microporous Mater.*, **2**, 17 (1993).

22) C-Y. Chen, S. L. Burkett, H-X. Li, and M. E. Davis, *Microporous Mater.*, **2**, 27 (1993).

23) a) Q. Huo, D. I. Margolese, U. Ciesla, P. Feng, T. E. Gier, P. Sieger, R. Leon, P. M. Petroff, F. Schuth, and G. D. Stucky, *Nature*, **368**, 317 (1994); b) Q. Huo, D. I. Margolese, U. Ciesla, D. G. Demuth, P. Feng, T. E. Gier, P. Sieger, A. Firouzi, B. F. Chmelka, F. Schuth, and G. D. Stucky, *Chem. Mater.*, **6**, 1176 (1994).

24) A. K. Pant and D. W. J. Cruickshank, *Acta Crystallogr., Sect. B*, **B24**, 13 (1968).

25) A. K. Pant, *Acta Crystallogr., Sect. B*, **B24**, 1077 (1968).

26) S. Inagaki, Y. Yamada, Y. Fukushima, and K. Kuroda, "In Studies in Surface Science and Catalysis 92, Science and Technology in Catalysis 1994," ed by Y. Izumi, H. Arai, and M. Iwamoto, Kodansha, Tokyo (1994), pp. 143—148.

27) S. Inagaki, Y. Fukushima, K. Kuroda, and K. Kuroda, *J. Colloid Interface Sci.*, in press.